

# Anthropogenic Influence on the Autocorrelation Structure of Hemispheric-Mean Temperatures

T. M. L. Wigley,\* R. L. Smith, B. D. Santer

It is shown that lagged correlations for and cross-correlations between observed hemispheric-mean temperature data differ markedly from those for unforced (control-run) climate model simulations. The differences can be explained adequately by assuming that the observed data contain a significant externally forced component involving both natural (solar) and anthropogenic influences and that the global climate sensitivity is in the commonly accepted range. Solar forcing alone cannot reconcile the differences in autocorrelation structure between observations and model control-run data.

Most attempts to identify a human influence on climate have searched for an anthropogenic signal either in temperature time series data (1) or in spatial patterns of temperature change (2, 3). Relatively few analyses have considered the lag-correlation (4) structure of temperature data, and such studies have done so only in the context of autoregressive-moving average (ARMA) or regression modeling (5). Here we consider the lag-correlation structure of hemispheric-mean temperatures directly. We show that the observed structure can only be explained by assuming the existence of a strong externally-forced component of temperature change. We also demonstrate that this external forcing is most likely to be composed of both natural (solar) and anthropogenic (greenhouse gas and aerosol) components.

We consider the correlations between Northern Hemisphere (NH) and Southern Hemisphere (SH) mean temperatures in year  $i$  ( $N_i$  and  $S_i$ ) and temperatures in the same or opposite hemisphere lagged by up to 20 years: that is,  $r(N_i, N_{i-n})$ ,  $r(S_i, S_{i-n})$  and  $r(N_i, S_{i-n})$  for  $n = -20$  to  $+20$  (4). The temperature data we use are observed data (6), model control-run (7) and perturbed-run (8) data from two coupled ocean/atmosphere general circulation models (O/AGCMs), and results from a simple upwelling-diffusion energy-balance model (9). Assuming that the O/AGCM control-run data provide a reasonable representation of the unforced behavior of the real climate system, then a marked difference between the observations and the control-run results would provide evidence of

external forcing effects in the observed temperature record.

Our analysis does, indeed, show striking differences between observed and control-run autocorrelations (Fig. 1). At all lags, the observed data show much stronger correlations than the two O/AGCM control runs. Both the observed data and the Geophysical Fluid Dynamics Laboratory (GFDL) control-run data (7) show larger lagged correlations in the SH than in the NH, as one might expect as a result of the larger ocean area and thermal inertia in the SH. The U.K. Hadley Centre (HadCM2) control simulation, however, shows larger autocorrelations in the NH than the SH: NH autocorrelations are similar to those in the GFDL run, but SH autocorrelations were much lower, pointing to large differences between the models in their SH behavior.

The observed and control-run differences in Fig. 1 cannot be a result of inadequate representation of the El Niño/Southern Oscillation (ENSO) influence in the models: as Fig. 1 shows, removing the ENSO influence from the observations (10) had only a marginal effect and did not bring the observed correlations into closer accord with the control-run results. We must therefore seek other explanations for these differences.

The control-run simulations considered only internally generated variability of the climate system. The differences in Fig. 1, therefore, can only be explained by gross errors in the observations, lack of realism of the model control runs, or the existence of external forcing effects in the observations. Many studies attest to the quality of the observed data (11). As for the models, there is no evidence to suggest that they underestimate the magnitude of internal variability on time scales of 20 to 100 years by the large amounts required to explain the Fig. 1 differences. The general agreement between the two independent models also suggests that

model errors are an unlikely explanation.

If external forcing (anthropogenic or natural or both) is the explanation for observed versus control-run differences, then removing external forcing effects from the observations should bring them into closer accord with the control-run results. The simplest possible model for an externally forced component is a linear trend in the observational data. After removal of best-fit linear trends in the individual NH and SH series, the residuals show autocorrelations that are similar to the unforced control-run data, except for anomalously high correlations between the two hemispheres when the SH leads the NH by 0 to 10 years (Fig. 1). These results suggest that the differences between the observations and results from the control-runs can be reconciled by the existence of some form of external forcing with a temperature response similar to a long-term linear trend.

A less ad hoc procedure for removing external forcing influences is to model their temperature effects deterministically with a simple climate model. We did this using the upwelling-diffusion (U-D) model of Wigley and Raper (9) as used by the Intergovernmental Panel on Climate Change (IPCC) (12). We considered the effects of both natural and anthropogenic forcing. The primary natural factors are volcanic activity and solar variability. Because demonstrated volcanic influences are both infrequent and short-term they may be rejected a priori as a possible explanation for the autocorrelation differences between the observed data and control-run results (13). We therefore consider only solar effects here using a recent reconstruction of solar irradiance changes (14). For anthropogenic forcing we consider both greenhouse-gas (ghg)-only and ghg-plus-aerosol forcing using IPCC forcing estimates (15).

Best-fit (optimized) estimates of solar, anthropogenic, and solar-plus-anthropogenic forcing effects were obtained by adjusting the U-D model's climate sensitivity (16) until the root-mean-square difference between modeled and observed global-mean temperatures was minimized (17). The best-fit sensitivities are: solar forcing alone,  $\Delta T_{2x} = 28^\circ\text{C}$ ; anthropogenic forcing alone,  $\Delta T_{2x} = 6.5^\circ\text{C}$ ; solar-plus-anthropogenic forcing,  $\Delta T_{2x} = 3.2^\circ\text{C}$  (18). The specific forcing cases are referred to below and in the figures as ANTH (anthropogenic forcing alone), SUN (solar forcing alone) and BOTH (solar and anthropogenic forcing together), with the qualifier "(OPT)" for cases where an optimum sensitivity was used or "(1.5)" or "(4.5)" when a specific sensitivity of  $1.5^\circ\text{C}$  or  $4.5^\circ\text{C}$  was used. Hemispheric-mean temperatures from these best-fit and specific-sensitivity results were then subtracted from the observed data. In all three optimized cases, ANTH(OPT), SUN(OPT), and BOTH(OPT), the autocorrelation structure of the residuals differs radically

T. M. L. Wigley, National Center for Atmospheric Research, Boulder, CO 80307, USA. R. L. Smith, Department of Statistics, University of North Carolina, Chapel Hill, NC 27599, USA. B. D. Santer, PCMDI, Lawrence Livermore National Laboratory, Livermore, CA 94550, USA.

\*To whom correspondence should be addressed. E-mail: wigley@ucar.edu

## REPORTS

from that for the raw observational data and becomes more similar to that for the unforced GCM control runs (Fig. 2). The best overall match with control-run results is obtained for the optimized “BOTH” case, when the combined effects of solar and anthropogenic forcing are subtracted from the observed data (Fig. 2).

For NH-NH and SH-SH correlations, subtraction of a model-based externally forced component gives results similar to those for linear trend subtraction. However, the trend-removal case is less constrained than the model-based case. In the former, best-fit trends are removed from the individual NH and SH time series independently. In the model-based case, the relative effects in each hemisphere are constrained a priori by model structure and inter-hemispheric forcing differences. For the NH-SH cross-correlations, model-based signal removal gives much better results than linear trend removal. These results imply that the externally forced component cannot be described adequately simply by fitting linear trends to the individual hemispheric-mean time series.

For the ANTH(OPT) and SUN(OPT) cases, the best fits require unrealistically high climate sensitivities. How dependent are the results on the value of the climate sensitivity? In the ANTH case, the autocorrelation results for the residuals (not shown here) are virtually unchanged if a realistic but high climate sensitivity is used ( $\Delta T_{2x} = 4.5^\circ\text{C}$ ). Within the uncertainty bounds of  $\Delta T_{2x}$  (16), therefore, subtraction of anthropogenic forcing alone provides a reasonable fit to the control-run autocorrelation structure (but not as good as if solar forcing is also included).

For solar forcing alone (SUN), the value of  $\Delta T_{2x}$  affects the results more noticeably. To illustrate this we compare the optimized case [SUN(OPT),  $\Delta T_{2x} = 28^\circ\text{C}$ ] with the SUN result for a realistic, but high sensitivity of  $\Delta T_{2x} = 4.5^\circ\text{C}$  [SUN(4.5)]. The SUN(OPT) and SUN(4.5) cases lead to NH-NH autocorrelations in the residuals that match the control-run results equally well for lags greater than 10 (Fig. 2A). However, for lower lags in the NH-NH case and for the SH-SH and NH-SH results in general, SUN(4.5) is markedly inferior to SUN(OPT) (Fig. 2A and 2B). This comparison implies that, unless the magnitude of the solar forcing component is much larger than that used here (14), solar forcing alone is insufficient to explain the behavior of the observed temperature data.

For anthropogenic-plus-solar forcing, the best-fit sensitivity ( $3.2^\circ\text{C}$ ) is within the accepted uncertainty range (16). For this case (“BOTH”) we consider the influence of climate sensitivity by using  $\Delta T_{2x} = 1.5^\circ\text{C}$  and  $\Delta T_{2x} = 4.5^\circ\text{C}$  to define the signal extracted from the observed data [BOTH(1.5) and BOTH(4.5)] and then compare the autocorrelations of their residuals with those for

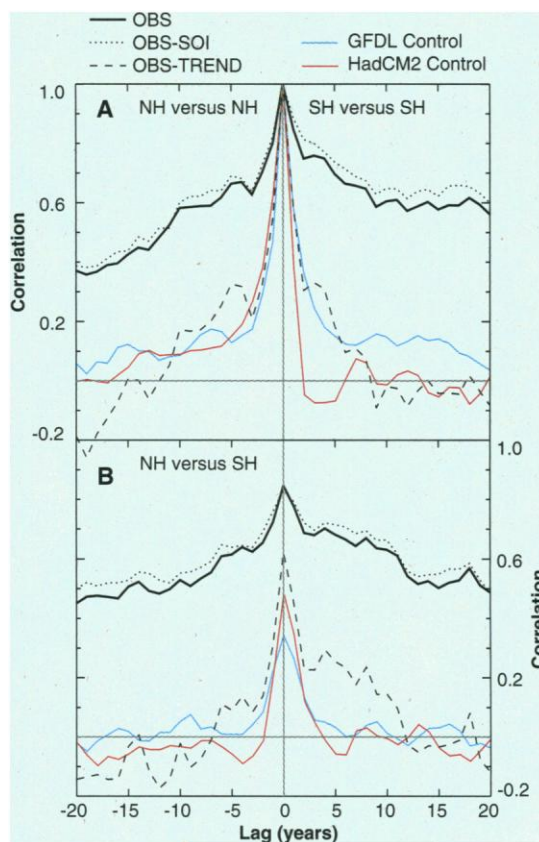


**Fig. 1.** General circulation model (GCM) control-run lagged correlations for and cross-correlations between hemispheric-mean temperatures in (A) NH versus NH and SH versus SH and (B) NH versus SH compared with results for raw observed data (OBS), observed data with the ENSO influence removed [using the Southern Oscillation Index, SOI, as an ENSO indicator—see (70)] (OBS-SOI), and observed data with linear trends removed (OBS-TREND). Note that the sign of the lag is irrelevant in the NH-NH and SH-SH cases. For the NH versus SH case (B), negative lags correspond to NH leading and positive lags correspond to SH leading. Control-run data are from the GFDL and U.K. Hadley Centre (HadCM2) models. The differences between the observed and control-run results are statistically significant (7).

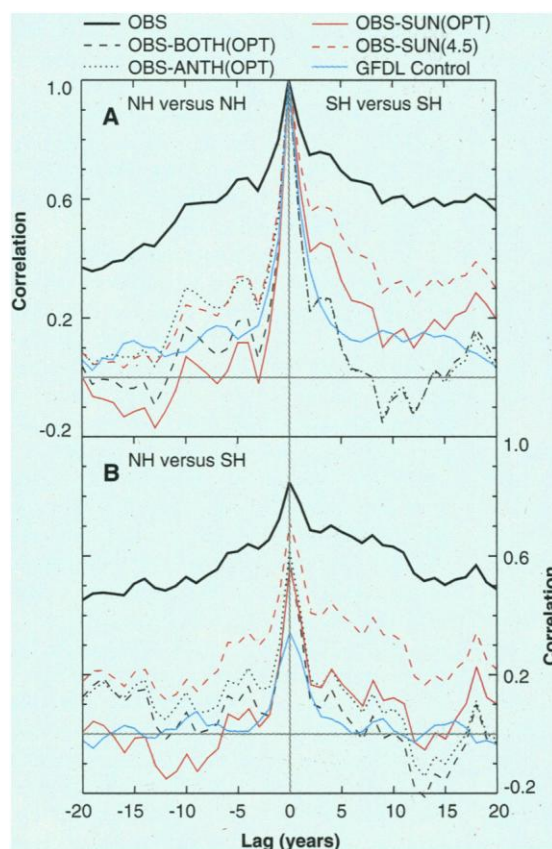


**Fig. 2.** Observed and GCM control-run (GFDL) lagged correlations compared with results for observed data after removing different external-forcing effects. Shown are a best-fit estimate of the influence of anthropogenic forcing [OBS-ANTH(OPT)]; best-fit and sub-optimal estimates of the influence of solar forcing [(OBS-SUN(OPT) and OBS-SUN(4.5);  $4.5^\circ\text{C}$ ) here refers to the climate sensitivity used in the sub-optimal case]; and a best-fit estimate of the influence of anthropogenic-plus-solar forcing [OBS-BOTH(OPT)]. (A) and (B) as in Fig. 1. Note that SUN(OPT) requires an unrealistically high climate sensitivity of  $28^\circ\text{C}$  to optimize the fit. For the NH versus SH case (B), negative lags correspond to NH leading and positive lags correspond to SH leading.

**Fig. 3 (left).** Observed and GCM control-run (GFDL) lagged correlations compared with results for observed data with combined anthropogenic-plus-solar forcing effects removed. The latter were calculated using climate sensitivities of 3.2°C [the best-fit case, denoted OBS-BOTH(OPT)], 4.5°C [OBS-BOTH(4.5)] and 1.5°C [OBS-BOTH(1.5)]. (A) and (B) as in Fig. 1. For the NH versus SH case (B), negative lags correspond to NH leading and positive lags correspond to SH leading.

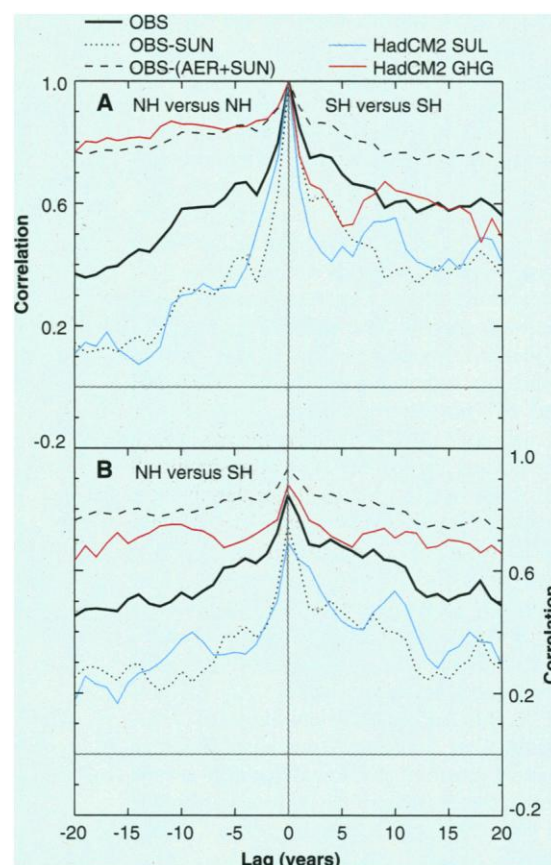
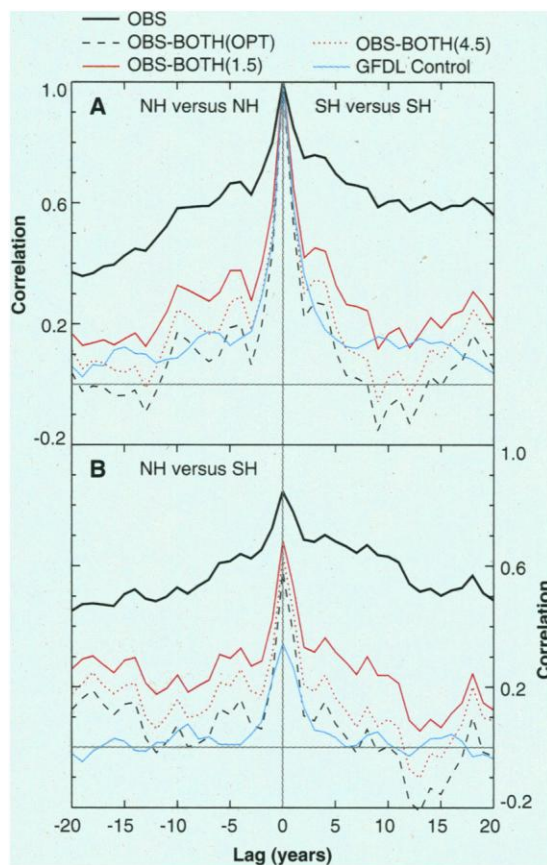


**Fig. 4 (right).** Lagged correlations for observed, adjusted-observed, and GCM (HadCM2) perturbation experiment data. For comparison with the HadCM2 SUL simulation, solar effects have been removed from the observed data (OBS-SUN); for comparison with the HadCM2 GHG simulation, solar plus effective aerosol effects (that is, combining tropospheric ozone and aerosol influences) were removed [OBS - (AER+SUN)]. (A) and (B) as in Fig. 1. For the NH versus SH case (B), negative lags correspond to NH leading and positive lags correspond to SH leading.

BOTH(OPT) (Fig. 3). Higher sensitivity [BOTH(4.5) in Fig. 3] leads to results that match the unforced control-run results almost as well as the best-fit case [BOTH(OPT)]. For low sensitivity (1.5°C) the match is less good. The similarity of these results means that it is not possible to use them to constrain the climate sensitivity any more than the current best-estimate range (1.5–4.5°C), especially given uncertainties in the forcing and in the autocorrelation structure of the unforced climate system. The results obtained here are, however, entirely consistent with a sensitivity within the accepted range and are noticeably degraded if a sensitivity outside this range is assumed.

The above interpretations assume that the GFDL and HadCM2 control runs simulate the unforced behavior of the climate system realistically. We can test how realistic the autocorrelation structure of these models is by examining how well they simulate known 20th-century climate changes when driven by estimates of external forcing. We illustrate this with results from two simulations with HadCM2 (8); one for forcing with CO<sub>2</sub> concentration changes alone (“GHG”), and another where combined CO<sub>2</sub> and albedo (as a proxy for direct sulfate aerosol) forcing was used (“SUL”). These model results cannot be compared directly with observations, however, because the observations are likely to

be influenced by other, additional forcing factors. We therefore need to subtract from the observations effects not considered in the GCM simulations, namely solar forcing and aerosol forcing for GHG, and solar forcing only for SUL (19). The autocorrelation structures for GHG and SUL can then be compared directly with these two sets of adjusted-observed data (Fig. 4).

For all cases, the autocorrelation structure of the adjusted-observed data differs markedly from that for the raw observed data: Removing solar effects decreases the correlations because the trend in the adjusted-observed data is reduced, whereas removing solar-plus-aerosol effects has the opposite effect (20). For the NH, the autocorrelation structures for adjusted-observed data agree well with the GCM data (Fig. 4A). For the SH-SH and NH-SH cases the SUL autocorrelation structures agree well with the appropriate adjusted-observed data (Fig. 4A and 4B). In these cases, however, the GHG autocorrelations are substantially below those for the corresponding adjusted-observed data.

It is not clear why the GHG case performs less satisfactorily than the SUL case. However, since this degradation only occurs in analyses involving the SH, it is possible that the unusual SH autocorrelation structure that HadCM2 exhibits in its control-run mode (see Fig. 1) is at

least part of the explanation. Apart from this anomaly, the GCM results compare well with appropriately adjusted observed data and show no evidence of deficiencies serious enough to question any of our results.

Our results imply that anthropogenic and solar forcing have both significantly affected global climate. They are also consistent with a climate sensitivity in the range derived independently from climate models and supported by other empirical analyses of observational data (17).

**References and Notes**

1. R. A. Madden and V. Ramanathan, *Science* **209**, 763 (1980); T. M. L. Wigley and P. D. Jones, *Nature* **292**, 205 (1981).
2. T. P. Barnett and M. E. Schlesinger, *J. Geophys. Res.* **92**, 14772 (1987); B. D. Santer, T. M. L. Wigley, P. D. Jones, *Clim. Dyn.* **8**, 265 (1993); B. D. Santer *et al.*, *ibid.* **12**, 77 (1995); G. C. Hegerl *et al.*, *J. Clim.* **9**, 2281 (1996).
3. B. D. Santer *et al.*, *Nature* **382**, 39 (1996); S. F. B. Tett, J. F. B. Mitchell, D. E. Parker, M. R. Allen, *Science* **274**, 1170 (1996).
4. By lag correlation we mean the product-moment correlation coefficient between variable  $X$  in year  $i$  ( $X_i$ ) and variable  $Y$  in year  $i-n$  ( $Y_{i-n}$ ), denoted  $r(X_i, Y_{i-n})$ .  $n$  may be positive ( $Y$  leading) or negative ( $X$  leading). When  $X = Y$ , these lag correlations are referred to as autocorrelations, terminology that we apply here to both the  $X = Y$  and  $X \neq Y$  cases.
5. W. A. Woodward and H. L. Gray, *J. Clim.* **6**, 953 (1993); *ibid.* **8**, 1929 (1995); R. S. J. Tol, *Theor. Appl. Climatol.* **49**, 91 (1994); R. K. Kaufmann and D. I. Stern, *Nature* **388**, 39 (1997).

6. We used the same observed data as IPCC, updated (P. D. Jones, personal communication). For sources, see: N. Nicholls *et al.*, in *Climate Change 1995: The Science of Climate Change*, J. T. Houghton *et al.*, Eds. (Cambridge Univ. Press, Cambridge, 1996), pp. 133–192. Our analyses span 1881–1996. The conclusions of this paper do not depend on the precise start or end points.
7. We use data from two 1000-year unforced simulations with coupled ocean/atmosphere general circulation models: the Geophysical Fluid Dynamics Laboratory (GFDL) model [S. Manabe and R. J. Stouffer, *J. Clim.* **9**, 376 (1996)]; and the U.K. Hadley Centre model (HadCM2) [S. F. B. Tett, T. C. Johns, J. F. B. Mitchell, *Clim. Dyn.* **13**, 303 (1997)]. For the control-run results we used the full areal coverage to define the hemispheric means. For the observed data, coverage is incomplete and tends to increase with time. To test whether such coverage differences affected our results, we masked the control-run data with typical observed coverages and re-computed the correlations. The results were similar to the full-coverage results. Standard errors associated with the sample autocorrelations are typically of the order 0.05 or smaller in the case of the model data, and in the range 0.1 to 0.15 for the observational data. These were calculated by applying standard asymptotic formulae for the variance of sample autocorrelations [for example, see, p. 342 of W. A. Fuller, *Introduction to Statistical Time Series*, (Wiley-Interscience, ed. 2, New York, 1996)]. In doing so, we assume that the true autocorrelations used for calculating the theoretical results are those estimated from the model data. The result that the standard errors are larger for the observed series than the model series reflects the difference in sample sizes (116 against 1000). These results were also checked from the model data using a resampling procedure, based on the empirical standard deviation of sample autocorrelations calculated from maximally overlapping 116-year subseries of the 1000-year model runs; this produced results consistent with the asymptotic formulae. The results show that the difference between sample autocorrelations for the observed and either of the control-run series are 2 to 3 times the standard errors for the observed series. On this basis we conclude that the two sets of autocorrelations are indeed significantly different.
8. From HadCM2 [T. C. Johns *et al.*, *Clim. Dyn.* **13**, 103 (1997); J. F. B. Mitchell and T. C. Johns, *J. Clim.* **10**, 245 (1997)]. In these simulations, which span the period 1861–2100, greenhouse-gas effects were modeled using observed CO<sub>2</sub> changes inflated to account for non-CO<sub>2</sub> greenhouse gases, and sulfate aerosol effects were modeled by using changes in surface albedo.
9. T. M. L. Wigley and S. C. B. Raper, *Nature* **357**, 293 (1992); S. C. B. Raper, T. M. L. Wigley, R. A. Warrick, in *Sea-Level Rise and Coastal Subsidence: Causes, Consequences and Strategies*, J. D. Milliman and B. U. Haq, Eds. (Kluwer, Dordrecht, Netherlands, 1996), pp. 11–45. Simulations run from 1765 through 1996. The model differentiates between land and ocean in each hemisphere and gives hemispherically-specific temperature change results.
10. P. D. Jones, *Clim. Mon.* **17**, 80 (1988); updated (P. D. Jones, personal communication).
11. Reviewed by C. K. Folland, T. R. Karl, K. Ya. Vinnikov, in *Climate Change. The IPCC Scientific Assessment*, J. T. Houghton, G. J. Jenkins, J. J. Ephraums, Eds. (Cambridge Univ. Press, Cambridge, 1990), pp. 195–238; C. K. Folland *et al.*, in *Climate Change 1992: The Supplementary Report to the IPCC Scientific Assessment*, J. T. Houghton, B. A. Callander, S. K. Varney, Eds. (Cambridge Univ. Press, Cambridge, 1992), pp. 135–170; and by N. Nicholls *et al.* (6).
12. A. Kattenberg *et al.*, in *Climate Change 1995: The Science of Climate Change*, J. T. Houghton *et al.*, Eds. (Cambridge Univ. Press, Cambridge, 1996), pp. 285–357.
13. We have, nevertheless, tested this by subtracting estimated volcanic effects for all known major eruptions from the observed data. The influence on the autocorrelation structure is negligible.
14. D. V. Hoyt and K. H. Schatten, *J. Geophys. Res.* **98**, 18895 (1994). Other reconstructions, such as by J. L. Lean, J. Beer, and R. Bradley [*Geophys. Res. Lett.* **22**, 3195 (1995)], are similar. The results presented here do not depend on which solar data set is used.
15. The forcings used in the U-D model are the estimates employed by IPCC (72). Greenhouse gases included are CO<sub>2</sub>, CH<sub>4</sub>, N<sub>2</sub>O, tropospheric and stratospheric ozone, and halocarbons. Aerosols included are the direct and indirect effects of sulfates and aerosols from biomass burning. Extensions beyond 1990 were made using the IS92a emissions scenario and observed CO<sub>2</sub> data. The IS92a scenario is the central “existing policies” scenario produced by IPCC in 1992 [J. A. Leggett, W. J. Pepper, R. J. Swart, in *Climate Change 1992: The Supplementary Report to the IPCC Scientific Assessment*, J. T. Houghton, B. A. Callander, S. K. Varney, Eds. (Cambridge Univ. Press, Cambridge, 1992), pp. 69–95]. The modifications made to this scenario are described in T. M. L. Wigley, *Geophys. Res. Lett.* **25**, 2285 (1998).
16. The climate sensitivity (that is, the sensitivity to external forcing) is the equilibrium global-mean warming per unit radiative forcing, commonly expressed as the global-mean warming for a doubling of the CO<sub>2</sub> concentration,  $\Delta T_{2\times}$ . The most likely range for  $\Delta T_{2\times}$  is 1.5–4.5°C [J. F. B. Mitchell *et al.*, in *Climate Change. The IPCC Scientific Assessment*, J. T. Houghton, G. J. Jenkins, J. J. Ephraums, Eds. (Cambridge Univ. Press, Cambridge, 1990), pp. 131–172] representing roughly the 90% confidence interval. The concept may be applied to any forcing. For example, the equilibrium global-mean warming for a 1% increase in solar irradiance ( $2.4 \text{ W/m}^{-2}$ ) would be  $2.4(\Delta T_{2\times}/\Delta Q_{2\times})$  where  $\Delta Q_{2\times}$  is the forcing for 2x CO<sub>2</sub> (approx.  $4 \text{ W/m}^{-2}$ ).
17. T. M. L. Wigley, P. D. Jones, S. C. B. Raper, *Proc. Natl. Acad. Sci. U.S.A.* **94**, 8314 (1997). Note that these climate sensitivities depend on the assumed magnitudes of anthropogenic and solar forcing. In particular, they vary considerably if the magnitude of aerosol forcing is altered within the (large) uncertainty range of this component.
18. These values differ slightly from those in (17) because we use a different optimization interval.
19. We do this by fitting the U-D model (8) results for anthropogenic-plus-solar forcing to the observations (best-fit sensitivity 3.2°C) and then disaggregating the hemispheric-mean modeled temperatures into their solar, effective sulfate aerosol (see below), and residual anthropogenic components. The “effective aerosol” response is the sum of responses to direct and indirect sulfate aerosol forcing and tropospheric ozone. HadCM2 considers only direct sulfate aerosol forcing. Because its magnitude and pattern are similar to the effective aerosol forcing used in the U-D model, we considered the two to be equivalent for the purposes of producing adjusted-observed data.
20. Solar-plus-aerosol forcing leads to cooling. Thus, removing this component gives residuals with a larger positive trend than in the raw data.
21. G. A. Meehl, G. J. Boer, C. Covey, M. Latif, R. J. Stouffer, *Eos* **78**, 445 (1997).
22. Supported by USDOE (T.M.L.W. and B.D.S.), NOAA (Award No. NA87GP0105 to T.M.L.W.) and NSF (DMS-9705166 to R.L.S.). Observed temperatures from P.D. Jones and D.E. Parker; control-run GCM data provided through the CMIP (27) project; SUL and GHG data provided by J.M. Gregory. NCAR is sponsored by the National Science Foundation.

16 September 1998; accepted 2 November 1998

## A Dielectric Omnidirectional Reflector

Yoel Fink, Joshua N. Winn, Shanhui Fan, Chiping Chen, Jurgen Michel, John D. Joannopoulos, Edwin L. Thomas\*

A design criterion that permits truly omnidirectional reflectivity for all polarizations of incident light over a wide selectable range of frequencies was used in fabricating an all-dielectric omnidirectional reflector consisting of multilayer films. The reflector was simply constructed as a stack of nine alternating micrometer-thick layers of polystyrene and tellurium and demonstrates omnidirectional reflection over the wavelength range from 10 to 15 micrometers. Because the omnidirectionality criterion is general, it can be used to design omnidirectional reflectors in many frequency ranges of interest. Potential uses depend on the geometry of the system. For example, coating of an enclosure will result in an optical cavity. A hollow tube will produce a low-loss, broadband waveguide, whereas a planar film could be used as an efficient radiative heat barrier or collector in thermoelectric devices.

Mirrors, probably the most prevalent of optical devices, are used for imaging and solar energy collection and in laser cavities. One can distinguish between two types of

mirrors, the age-old metallic and the more recent dielectric. Metallic mirrors reflect light over a broad range of frequencies incident from arbitrary angles (that is, omnidirectional reflectance). However, at infrared and optical frequencies, a few percent of the incident power is typically lost because of absorption. Multilayer dielectric mirrors are used primarily to reflect a narrow range of frequencies incident from a particular angle or particular angular range. Unlike their metallic counterparts, dielectric reflectors can be extremely low loss. The ability to reflect light of arbitrary angle of incidence for all-dielectric structures has been associated with the existence of a

Y. Fink, Department of Material Science and Engineering and Plasma Science and Fusion Center, Massachusetts Institute of Technology, Cambridge, MA 02139, USA. J. N. Winn, S. Fan, J. D. Joannopoulos, Department of Physics, Massachusetts Institute of Technology, Cambridge, MA 02139, USA. C. Chen, Plasma Science and Fusion Center, Massachusetts Institute of Technology, Cambridge, MA 02139, USA. J. Michel and E. L. Thomas, Department of Material Science and Engineering, Massachusetts Institute of Technology, Cambridge, MA 02139, USA.

\*To whom correspondence should be addressed.